Infra-red spectral microscopy of standing-wave resonances in single metal-dielectric-metal thin-film cavity

Janardan Nath[*a], Deep Panjwani[a], Farnood Khalilzadeh-Rezaie[a], Mehmet Yesiltas[a], Evan M. Smith[a,b], James C. Ginn[b], David J. Shelton[b], Carol Hirschmugl[c], Justin W. Cleary[d], and Robert E. Peale[a]

[a]Department of Physics, University of Central Florida, Orlando, 32816, USA; [b]Plasmonics, Inc., 12605 Challenge Pkwy STE 150, Orlando FL 32826, USA; [c]Department of Physics, University of Wisconsin, Milwaukee, WI 53211, USA; [d]Sensors Directorate, AFRL, Wright Patterson AFB, Dayton, OH 45433, USA

ABSTRACT

Resonantly absorbing thin films comprising periodically sub-wavelength structured metal surface, dielectric spacer, and metal ground plane are a topic of current interest with important applications. These structures are frequently described as "metamaterials", where effective permittivity and permeability with dispersion near electric and magnetic resonances allow impedance matching to free space for maximum absorption. In this paper, we compare synchrotron-based infrared spectral microscopy of a single isolated unit cell and a periodic array, and we show that the resonances have little to do with periodicity. Instead, the observed absorption spectra of usual periodically structured thin films are best described as due to standing-wave resonances within each independent unit cell, rather than as due to effective optical constants of a metamaterial. The effect of having arrays of unit cells is mainly to strengthen the absorption by increasing the fill factor, and such arrays need not be periodic. Initial work toward applying the subject absorbers to room-temperature bolometer arrays is presented.

Keywords: Metamaterial absorbers, Infra-red (IR), Mid-IR, Synchrotron radiation, diffraction limited IR imaging.

1. INTRODUCTION

Thin film "metamaterial" absorbers have gained attention recently for various applications such as photo-voltaics[1], thermovoltaics[2], terahertz and thermal imaging[3], stealth technology[4], sensing[5] and IR emitters[6]. Resonant absorption up to 99% in such films has been demonstrated in the UV[7], visible[7], near-IR[8], mid-IR[9], Long-Wave-IR[7], terahertz[3] and gigahertz[10] spectral regions. These structured films are usually much thinner than their resonance wavelengths,[10] and the periodicity of the structures that comprise them is similarly sub-wavelength. Independence on polarization and incidence angle have been demonstrated[11-15].

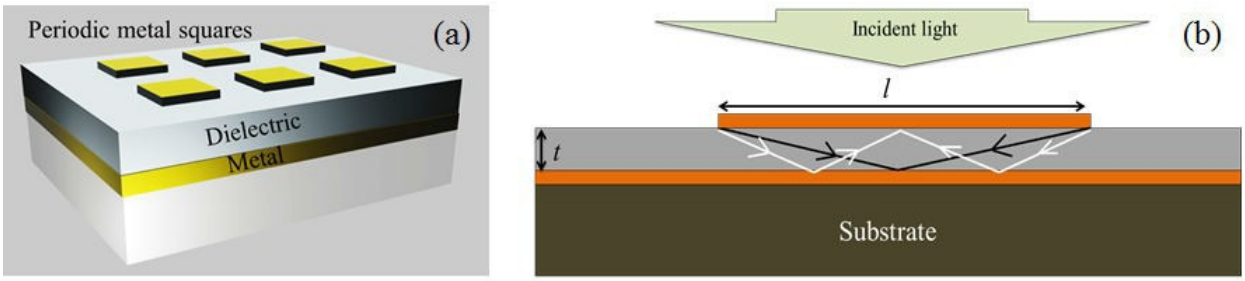

Fig. 1. (a) Schematic of structured thin-film absorber comprising periodic metal squares on dielectric spacer on metal ground plane on substrate. (b) Schematic diagram of one unit cell of the structure. Standing waves with odd numbers *b* of lateral reflections are indicated.

*janardan..nath@knights.ucf.edu

Metamaterials, Metadevices, and Metasystems 2015, edited by Nader Engheta, Mikhail A. Noginov, Nikolay I. Zheludev, Proc. of SPIE Vol. 9544, 95442M

Structured thin-film absorbers typically comprise 3 layers, namely a top surface metal with sub-wavelength patterning, a dielectric spacer, and a metal ground plane on suitable substrate[3-15]. Patterning is usually periodic and unit cells can have various geometries, e.g. split ring resonators, squares, rectangles, or circles. At wavelengths shorter than far-infrared, simpler patterns are favored for ease of fabrication. Fig. 1 presents a schematic of such a pattern comprising a periodic array of squares.

The subject structured films are frequently considered as "meta-materials", meaning the response is determined according to macroscopic electrodynamics, where the sub-wavelength structures result in effective permittivity and permeability. Electric and magnetic resonances[3,6,8,12] create strong dispersion that allows matching of the surface impedance to that of free space, a condition for strong absorption. The vast majority of papers in this field make no attempt to calculate the effective optical constants analytically, relying instead on numerical electrodynamic calculations to simulate the conditions and results of experiment. Thus, the meta-material picture provides mainly a qualitative understanding of the observed effects. Alternative theories are also reported such as interference theory[13] and planar wave-guide model[14], which are based on optical standing waves rather than magnetic resonances. We showed that such a standing wave model well explained far-infrared results based on a structure like that in Fig. 1.[15] Successes of the model included prediction of the fundamental and higher order resonance wavelengths, the dependence of these resonances on square size and dielectric thickness, the independence of the resonances on the period of the structure, and the insensitivity to polarization or incidence angle.[15] Our calculations supposed that each unit cell acts independently, with no dependence of resonance wavelength on the structure's period.

An objective of this work was to experimentally demonstrate the predicted independence of resonance wavelength on period. To do this, we fabricated a structure comprising a single unit cell having only a single isolated square. Then we determined the spatial distribution of absorption by synchrotron-based infrared spectral reflection microscopy. The absorption spectrum at the center of the square was then compared to the spectrum of a periodic array of such squares. The resonance wavelengths are the same. The main effect of any interaction between squares was that the quality factor of the resonance for the array was very slightly smaller. That the absorption of the isolated square was weaker we attribute to the smaller fill factor compared to the periodic array.

2. THEORY

Standing wave resonances in the dielectric under each surface square (Fig. 1b) explain the positions of a series of resonances in our films.[15] Incident light polarizes the squares, resulting in edge dipoles that are secondary sources of radiation, which can propagate evanescently under the squares. The resonance wavelength is given by,

$$\lambda(b,m) = \frac{2(b+1)n(\lambda)}{b+2m}\sqrt{t^2 + l^2/(b+1)^2}\,, \tag{1}$$

where m = 0, 1, 2, 3,… and b = 1, 3, 5,… represents an odd number of reflections (bounces) from the metals. The fundamental resonance m = 0 for b = 1 is

$$\lambda(1,0) = 4n(\lambda)\sqrt{t^2 + l^2/4}\,. \tag{2}$$

Similarly, for b = 3, the fundamental m = 0 is given by,

$$\lambda(3,0) = \frac{8n(\lambda)}{3}\sqrt{t^2 + l^2/16}\,. \tag{3}$$

and for m = 1, b = 1 we have

$$\lambda(1,1) = \frac{4n(\lambda)}{3}\sqrt{t^2 + l^2/4}. \quad (4)$$

These formulas agree very well with resonances observed experimentally and by numerical simulation at far-IR wavelengths for samples with periodic arrays of squares.[15]

3. EXPERIMENTAL DETAILS

We fabricated samples for the mid-IR range comprising isolated squares of lateral dimension 1.5 – 2.2 microns patterned on 100 nm thick SiO_2 on 200-nm-thick gold on silicon. For comparison, we also prepared an array with 3.2 μm period of 2.2 μm squares, and the same dielectric and ground plane layers. The absorber has the 3 layer structure shown schematically in Fig. 1. First, electron-beam evaporation was used to deposit 10 nm of Cr on a Si wafer followed by 200 nm of gold, 10 nm of Cr, and 100 nm of SiO_2, all without breaking vacuum. The thickness monitor was calibrated on witness samples by step profilometry. Isolated squares of from 1.5 to 2.2 μm lateral dimension and 150 nm thickness were patterned by electron beam lithography, sputtering, and metal lift-off. The separation between squares was at least 10 μm. Periodic arrays of squares with total area 300 μm x 300 μm were also patterned on a different part of the wafer.

The InfraRed ENvironmental Imaging (IRENI) beam line at the (former) Synchrotron Radiation Center (SRC) of the University of Wisconsin was used to obtain infrared reflectance spectra[16,17]. Multiple beams were combined to achieve high brightness up to ~1000 times more than provided by the usual globar source.[16] A Brucker Vertex FTIR spectrometer equipped with a Hyperion 3000 infra-red microscope (20x Schwarzschild objective, 0.65 numerical aperture) and a 128 x 128 pixel focal-plane-array detector was used to collect data over the 900 - 3700 cm^{-1} spectral range (2.7 - 11.1 μm wavelength) with 4 cm^{-1} spectral resolution. IRidys (Infrared Imaging and Data Analysis) software was used to extract data from different pixels. The individual pixel size in the FPA is 0.54 microns x 0.54 microns.[16,17] For NA = 0.65, at 2.7 microns wavelength, the diffraction limit d = 2.1 μm using the Abbe criterion.[37] Hence, diffraction limited imaging was achieved over the entire spectral range. The cone of incidence angles was determined from the NA with n = 1 to be 40.5 degrees. Absorptance A is found from $A = 1 - R$, since transmission $T = 0$ due to the optically thick gold ground plane. Since the structure size is much smaller than the operating wavelength, scattering is assumed to be negligible.

The refractive index of electron-beam evaporated SiO_2 was measured from 1 to 40 μm wavelength using an IR-VASE ellipsometer on a 1.6-μm-thick layer deposited on 150-nm-thick gold on polished Si.

4. RESULTS

Fig. 2 presents IR micro-spectroscopy for a single isolated square l = 2.1 μm and t = 0.1 μm. Fig. 2(a) presents an SEM image of the square. Fig. 2(b) presents an IR image of the isolated square at 6.3 μm wavelength, where the dimension appears more than twice larger than the physical dimension due to diffraction. Fig. 2(c) presents the method of graphically solving Eqs. (2) – (3) for the resonance wavelengths for $\lambda(1, 0)$, $\lambda(3, 0)$ and $\lambda(1, 1)$. The black data curve represents the measured refractive index spectrum n for evaporated SiO_2. Sample parameters are l = 2.1 μm and t = 0.1 μm. Red, blue and green straight lines represent Eqs. (2) – (4) solved for $n(\lambda)$. The intersections of straight lines with index spectrum solves for the resonance wavelengths. The fundamental resonance $\lambda(1, 0)$ is obtained at 5.7 μm wavelength. The $\lambda(3, 0)$ and $\lambda(1, 1)$ solutions nearly coincide at 2.1 μm wavelength.

Fig. 2(d) presents the reflectance spectrum at the centermost pixel from the IR image of the square in Fig. 2(b), where the absorption is strongest. Two prominent absorption features are observed, at 6.3 and 2.5 μm wavelength, which are identified as $\lambda(1, 0)$ and $\lambda(3, 0)$ resonances, respectively. Dashed vertical lines represent the theoretically calculated resonances. The difference between measured and predicted wavelengths is 10%.

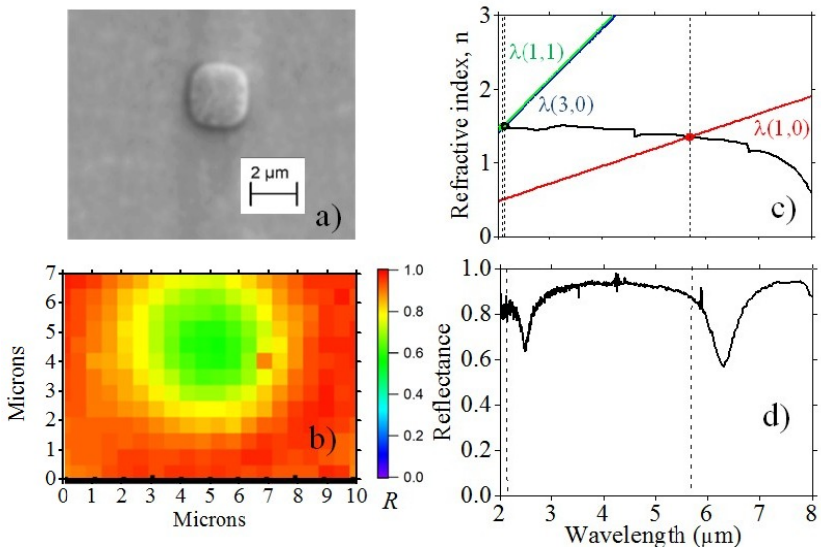

Figure 2. IR micro-spectroscopy of single isolated unit cell. a) SEM image of surface square; b)IR image at 6.3 μm wavelength; c) graphical solution for resonance wavelengths λ(1, 0), λ(3, 0), and λ(1, 1). d) reflectance spectrum from a pixel at the middle of the square in the IR image.

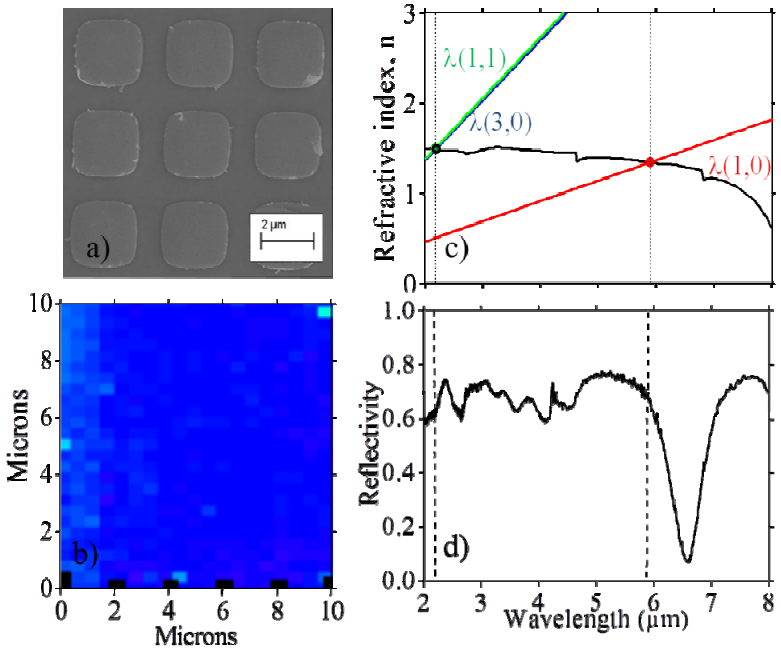

Figure 3. Synchrotron IR micro-spectroscopy imaging data of square array. a) SEM image of the array; b) IR image of the array at 6.6 μm wavelength; c) graphical solution of resonance wavelengths for λ(1, 0), λ(3, 0) and λ(1, 1); (d) reflectance spectrum from one pixel. Dashed horizontal lines represent theoretical resonances.

Figs. 3(a)-(d) present IR micro-spectroscopy for the array of squares. Fig. 3(a) presents an SEM image of a portion of the array. Fig. 3(b) presents the IR image for the same field of view at 6.6 μm wavelength, where the color scale is the same as in Fig. 2, indicating nearly uniform absorption across the array. Fig. 3(c) represents graphical solution of resonance wavelengths for $\lambda(1, 0)$, $\lambda(3, 0)$ and $\lambda(1, 1)$ according to Eqs. (2)-(4), which differs slightly from the corresponding plot in Fig. 2 because of slightly larger square dimension ($l = 2.2$ μm). The fundamental resonance $\lambda(1, 0)$

is obtained at 5.9 μm wavelength. The $\lambda(3, 0)$ and $\lambda(1, 1)$ nearly coincide at 2.2 μm. Fig. 3(d) presents the reflectance spectrum from one pixel. Dashed vertical lines represent theoretically calculated resonances. A 93% deep $\lambda(1, 0)$ fundamental absorption appears at 6.7 μm wavelength.

Table 1: Comparison of resonance wavelengths.

	Sample parameters (μm)	Theoretical wavelength (μm)	Experimental wavelength (μm)	Difference (%)
Single square	$l = 2.1$, $t = 0.1$	$\lambda(1,0)=5.7$ $\lambda(3,0)=2.1$	$\lambda(1,0)=6.3$ $\lambda(3,0)=2.5$	*10* *17*
Periodic array	$l = 2.2$, $t = 0.1$	$\lambda(1,0)=5.9$ $\lambda(3,0)=2.2$	$\lambda(1,0)=6.7$ $\lambda(3,0)=2.6$	*15* *17*

Fig. 4 presents an SEM image of a single pixel of a room-temperature bolometer array, showing that the transition from the basic research presented here to practical devices is underway. Fabrication details were presented in refs. 18 and 19. The bolometer dimension is only ~30 μm, i.e. about 3 times larger than the intended wavelength, so that only a 4x4 array of squares can be accommodated. Nevertheless, the spectral microscopy presented in Fig. 3 shows that such an array is sufficient to produce a strong and spatially uniform absorption over the entire surface. Characterization of the LWIR response and noise is underway, as was done for gold-black absorber on the same type of bolometer.[17]

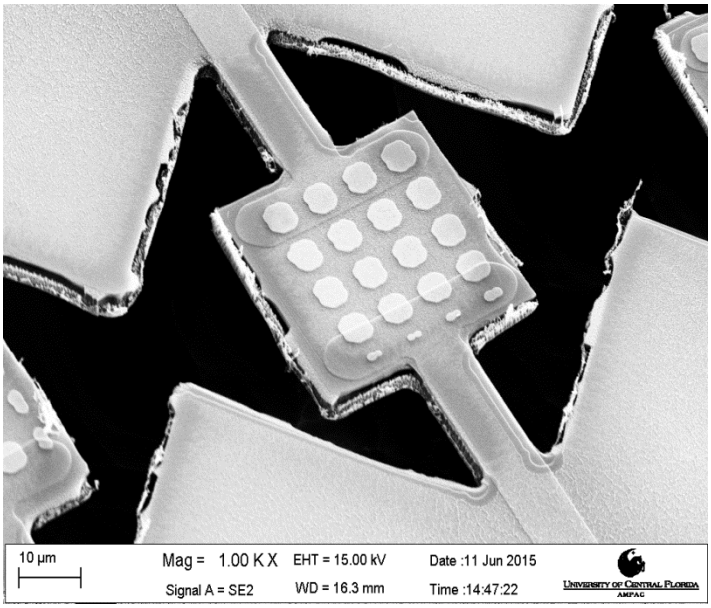

Fig. 4. SEM image of one pixel from a linear array of VO_x air-bridge bolometers, each coated with array of LWIR resonant absorbers.

5. DISCUSSION

Comparison of Fig. 2d and Fig. 3d shows that the main difference in the fundamental absorption is the strength, which can be attributed to the difference in fill factor. Closer inspection shows that the fundamental for the array is at slightly longer wavelength, which can be attributed to the slightly larger square size. Table 1 collects quantitative values for comparison. The absence of a strong difference in the positions of the resonances for single square and array of squares suggests that the squares absorb independently with little interaction. Thus, only dimensions within a single unit cell, and not the period of any array of cells, is important in defining the resonance frequency. It is difficult to think of a single square as a comprising a meta-material. A better description in that case would be absorption by a defect.

Regarding the position and strength of the higher order resonances, there is an oscillation in the baseline of the short-wave part of the array spectrum. This oscillation appears to be an artifact. Analysis of the spacing shows that for this to be Fabry-Perot oscillations due to an oxide layer on the sample, that layer would have to be 13 μm thick. No such layer can be present. Such an oscillation can occur if there is a noise spike in the interferogram that is offset from the usual centerburst. A peak in this baseline oscillation nearly coincides with the $\lambda(3,\ 0)$ absorption at 2.6 μm wavelength to make that absorption appear artificially weak and broad.

Returning to the Table 1 data for the fundamental, we see that the peak for the array is more redshifted with respect to theory than is the peak for the single square. This confirms our observation from simulated spectra as function of period, that when the squares are very close, a slight redshift appears for the fundamental due to couplings with next neighbors that increase the inertia of the oscillators.[15]

The resonance positions reported here for mid-IR devices agree with the theory less well than they did for our far-IR devices.[15] We note that the two classes of device are not simply scaled replicas of each other. The ratio $\lambda(1,0):t$ is 67 in the far-IR device but only 18 in the mid-IR device. Thus, coupling between square and ground plane will be correspondingly stronger for the mid-IR device, resulting in effects unaccounted for in our simple ray-diagram resonance model. For instance, surface plasmons must certainly be part of the mode description in the dielectric under the plate, with interaction between fields of plasmons bound to one plate interacting and being loaded by charges on the opposite plate.[20-23] Ultra-thin absorbers designed for the visible show resonance redshifts with decease in dielectric thickness.[8]

Besides the effect of fill factor to explain the relative weakness of the isolated square absorption, diffraction must additionally cause an apparent weakening. The actual absorption that occurs at the center of the square is spread-out over the diffraction spot, which has 4 times the area of the actual square. Were all the absorption in the diffraction spot integrated and confined to the area of the square, the absorption at its center would be corresponding stronger.

6. SUMMARY

We report IR micro-spectroscopy that shows the absorption resonances of thin structures comprising periodically patterned metal on dielectric on metal ground plane occurs within each unit cell independently. The resonance wavelengths are determined mainly by the geometrical parameters within each unit cell, independent of the period of the array. Thus, the periodic structures are better described as a collection of independent "defect" absorbers where the strength of the absorption depends primarily on fill factor than as "metamaterials" whose effective optical constants in a macroscopic electrodynamics description depend on appropriate averaging over dimensions much larger than the wavelength.

ACKNOWLEDGMENTS

UCF authors acknowledge partial support from the Florida High Technology Corridor (I-4) program. J. W. C. was supported by Air Force Office of Scientific Research under AFOSR LRIR No. 12RY10COR (Program Officer Dr. Gernot Pomrenke). R. E. P. was partially supported by Sensors Directorate at the Air Force Research Labs.

REFERENCES

[1] A. Vora, J. Gwamuri, N. Pala, A. Kulkarni, J. M. Pearce, and D. Ö. Güney, "Exchanging ohmic losses in metamaterial absorbers with useful optical absorption for photovoltaics," Scientific reports 4, 4901 (2014).
[2] C. Simovski, S. Maslovski, I. Nefedov, and S. Tretyakov, "Optimization of radiative heat transfer in hyperbolic metamaterials for thermophotovoltaic applications," Optics express 21, 14988 (2013).
[3] H. Tao, N. I. Landy, C. M. Bingham, X. Zhang, R. D. Averitt, and W. J. Padilla, "A metamaterial absorber for the terahertz regime: Design, fabrication and characterization," Optics express 16, 7181 (2008).
[4] A. K. Zadeh and A. Karlsson, "Capacitive circuit method for fast and efficient design of wideband radar absorbers," IEEE Transactions on Antennas and Propagation 57, 2307 (2009).
[5] N. Liu, M. Mesch, T. Weiss, M. Hentschel, and H. Giessen, "Infrared perfect absorber and its application as plasmonic sensor," Nano letters 10, 2342 (2010).
[6] M. Diem, T. Koschny, and C. M. Soukoulis, "Wide-angle perfect absorber/thermal emitter in the terahertz regime," Physical Review B 79, 033101 (2009).

[7] J. Nath, D. Maukonen, E. Smith, P. Figueiredo, G. Zummo, D. Panjwani, R. E. Peale, G. Boreman, J. W. Cleary, and K. Eyink, "Thin-film, wide-angle, design-tunable, selective absorber from near uv to far infrared," Proc SPIE 87041D, (2013).
[8] J. Hao, L. Zhou, and M. Qiu, "Nearly total absorption of light and heat generation by plasmonic metamaterials," Physical Review B 83, 165107 (2011).
[9]J. Hendrickson, J. Guo, B. Zhang, W. Buchwald, and R. Soref, "Wideband perfect light absorber at midwave infrared using multiplexed metal structures," Optics letters 37, 371 (2012).
[10] H. Li, L. H. Yuan, B. Zhou, X. P. Shen, Q. Cheng, and T. J. Cui, "Ultrathin multiband gigahertz metamaterial absorbers," Journal of Applied Physics 110, 014909 (2011).
[11] L. Li, Y. Yang, and C. Liang, "A wide-angle polarization-insensitive ultra-thin metamaterial absorber with three resonant modes," Journal of Applied Physics 110, 063702 (2011).
[12] Y. Q. Ye, Y. Jin, and S. He, "Omnidirectional, polarization-insensitive and broadband thin absorber in the terahertz regime," JOSA B 27, 498 (2010).
[13] H.-T. Chen, "Interference theory of metamaterial perfect absorbers," Optics express 20, 7165 (2012).
[14] X.-Y. Peng, B. Wang, S. Lai, D. H. Zhang, and J.-H. Teng, "Ultrathin multi-band planar metamaterial absorber based on standing wave resonances," Optics express 20, 27756 (2012).
[15] J. Nath, S. Modak, I. Rezadad, D. Panjwani, F. Rezaie, and R. E. Peale, "Far-infrared absorber based on standing-wave resonances in metal-dielectric-metal cavity," Optics Express, accepted, in press (2015).
[16] M. J. Nasse, B. Bellehumeur, S. Ratti, C. Olivieri, D. Buschke, J. Squirrell, K. Eliceiri, B. Ogle, C. S. Patterson, M. Giordano, *et al.*, "Opportunities for multiple-beam synchrotron-based mid-infrared imaging at IRENI," Vibrational Spectroscopy 60, 10 (2012).
[17] M. J. Nasse, M. J. Walsh, E. C. Mattson, R. Reininger, A. Kajdacsy-Balla, V. Macias, R. Bhargava, and C. J. Hirschmugl, "High-resolution fourier-transform infrared chemical imaging with multiple synchrotron beams," Nature Methods 8, 413 (2011).
[18] Evan M. Smith, James C. Ginn, Andrew P. Warren, Christopher J. Long, Deep Panjwani, Robert E. Peale, David J. Shelton, "Linear bolometer array using a high TCR VOx-Au film," Proc. SPIE 9070, 120 (2014).
[19] Evan M. Smith, Deep Panjwani, James Ginn, Andrew Warren, Christopher Long, Pedro Figuieredo, Christian Smith, Joshua Perlstein, Nick Walter, Carol Hirschmugl, Robert E. Peale, and David Shelton, "Enhanced performance of VOx-based bolometer using patterned gold black absorber," Proc. SPIE 9451, 52 (2015).
[20] R. Peale, H. Saxena, W. Buchwald, G. Aizin, A. Muravjov, D. Veksler, N. Pala, X. Hu, R. Gaska, and M. Shur, "Grating-gate tunable plasmon absorption in InP and GaN based HEMTs," Proc. SPIE 74670Q (2009).
[21] H. Saxena, R. Peale, and W. Buchwald, "Tunable two-dimensional plasmon resonances in an InGaAs/InP high electron mobility transistor," Journal of Applied Physics 105, 113101 (2009).
[22] N. N. Esfahani, C. J. Fredricksen, G. Medhi, R. E. Peale, J.vW. Cleary, W. R. Buchwald, H. Saxena, and O. J. Edwards, "Plasmon resonance response to millimeter-waves of grating-gated InGaAs/InP HEMT," Proc. SPIE 80230R (2011).
[23] N. N. Esfahani, R. E. Peale, W. Buchwald, C. J. Fredricksen, J. Hendrickson, and J. W. Cleary, "Millimeter-wave photoresponse due to excitation of two-dimensional plasmons in InGaAs/InP high-electron-mobility transistors," Journal of Applied Physics 114, 033105 (2013).